Electrical imaging of the northern part of Lakshdweep Islands

P. B. V. Subba Rao* and A. K. Singh

Indian Institute of Geomagnetism, Panvel, Navi Mumbai 410 218, India

Magnetovariational fields recorded by an array of magnetometers in five different Lakshdweep Islands were analysed to infer the subsurface structure of the region. Only nighttime magnetovariational fields were used because of the prevailing uniform source field conditions. Transfer functions showing the relationship between vertical and horizontal magnetic field components were computed for a period range of 8–128 min using robust regression analysis. Observed induction pattern at all stations is dominated by island effect. Two-dimensional modelling across the northern part of the Chagos–Laccadive Ridge (CLR) brings out midcrustal conductivity anomaly associated with magmatic intrusions/fluids along the track of Reunion hotspot. This anomaly could be delineated after eliminating the shielding effect due to seawater column using 3-D thin sheet approximation. Conductivity anomaly may be associated with massive intrusions due to hotspot volcanism, during the northward drift of Indian plate over the Reunion mantle plume.

Keywords: Conductivity anomaly, Lakshdweep Islands, magnetovariational studies, Reunion hotspot.

HOTSPOTS and mid-ocean ridges are two major surface manifestations of mantle upwelling and magma generation on Earth. Hotspots are the regions of elevated topography spanning hundreds to thousands of kilometres that are capped with volcanoes. Hotspots are considered to result from buoyant upwelling of anomalously hot convection plumes arising from the deep mantle[1,2]. In plume–lithosphere interactions, partial melting of large plume head and/or hydrothermal circulation propagating through fissures and fractures can significantly enhance the electrical conductivity of the medium. Therefore, knowledge of electrical conductivity distribution can provide independent constraints in tracing the plume–lithosphere interactions.

Conductivity anomalies have been inferred by analysing the anomalous signatures in the transient geomagnetic field components through the principle of geomagnetic depth sounding (GDS)[3,4]. A large scale magnetometer array (including permanent observatories) in south India helped to locate the anomalous conductive structures in Palk Strait and underneath the Commorin Ridge[5–7]. Integration of regional magnetometer array over Indian Peninsula as well as supplemented by the ocean bottom magnetometer deployed in the Bay of Bengal mapped a major regional scale conductivity anomaly centred immediately south west (SW) of southern tip of India (SIOCA: south Indian offshore conductivity anomaly)[8].

The Chagos–Laccadive Ridge (CLR) is an aseismic ridge in the Indian Ocean that formed by the action of the Reunion hotspot. Drilling results from the Ocean Drilling Programme (ODP) sites suggest that the CLR was formed by processes associated with the Reunion plume[9]. The CLR extends more than 2500 km (north–south) on the western side of India into the Indian Ocean basin. The Lakshdweep group of islands occupy the northern part of the CLR.

Regional GDS survey was carried out in Lakshdweep and surrounding islands (station locations are shown in Figure 1) during April–May 2004. The thin sheet modelling of induction pattern (in terms of distribution of depth integrated conductance) has brought out high conductivity anomaly associated with the track of the Reunion hotspot[10]. This paper presents a more detailed 2-D model of the electrical conductivity anomaly associated with CLR.

Geology and tectonics of the area

The SW continental margin of India comprises several tectonic features that include CLR, Pratap Ridge and chain of grabens filled with sediments bordering the west coast of India. CLR is a prominent topographic feature, over which the Laccadive (Lakshdweep), Maldives and Chagos group of islands have formed. The Lakshdweep group of islands forms the northern part of CLR and is parallel to the western margin of India. Various hypotheses have been postulated for the evolution of CLR. Northern part of CLR is a fragment of the Indian continent[11–13] and old transform fault[14,15]. Recent studies[16] suggest that the northern part of the ridge formed a transition between continental crust and oceanic crust to the east and west respectively.

The findings of the ODP Leg 115 support that CLR is the inactive and subsided part of a linear volcanic feature, formed during the northward motion of the Indian plate

*For correspondence. (e-mail: srao@iigs.iigm.res.in)

over the Reunion hotspot[17–19]. A huge eruption of this hotspot around 65 Ma has led to the Deccan volcanism and separated Seychelles Plateau from India.

Analysis of magnetometer array data is described here. Detailed review of data processing techniques are given in refs 3, 20 and 21.

Data collection and processing

For data acquisition, Magson fluxgate magnetometers were deployed at five different islands as shown in Figure 1 and data were collected during April–May 2004 with a sampling interval of about 10 s.

Magnetograms

In magnetometer array studies, the physical quantities measured are the time-varying geomagnetic field, generally two horizontal components (*X*-northward positive and *Y*-eastward positive) and the vertical component (*Z*-positive downward). These time-varying fields have their origin in electric currents in and beyond ionosphere resulting from complex interactions of radiations and plasma flux from the Sun with the Earth's magnetosphere–ionosphere.

Some idea on the nature of conductivity distribution in the area under investigation can be obtained by the examination of stacked magnetograms of selected disturbance events in time domain. This is due to the fact that the variations in the vertical magnetic field are most indicative of lateral conductivity inhomogeneity as such inhomogeneity produces phase shifts and phase reversals in *Z* between two sites. If there were no lateral variations, during uniform source, one would expect no appreciable change in *X* and *Y* components and negligible amplitude would be observed in *Z* variations.

Magnetograms representative of a current concentration anomaly are shown in Figure 2 for the substorm event recorded on 5 May 2004. From the stacked plot, it can be seen that the amplitude of *Z*-variations is suppressed at Minicoy (MIN) and Bangaram (BAN). Though there are no pronounced spatial latitudinal variations in *X* and *Y*, strong changes exist at BAN and Amini (AMI). Such variations can be used to distinguish the situations arising due to the lateral inhomogeneities.

Spectral analysis

The observed anomaly over a station is integrated response of different conductive subsurface layers with lateral inhomogeneities; it is always desirable to have separate response of each layer in order to estimate its electrical parameter. Depth penetration of the induced currents being function of frequency, this is achieved by examining the observed variations in frequency domain. Digitized magnetic variation data (*X*, *Y* and *Z*) are chosen for time period (t) with sampling interval Δt. The requirement is that, the signal should have negligible spectral energy at periods shorter than twice the sampling interval (i.e. at all frequencies above the Nyquist frequency). The fast Fourier transform (FFT) of each component is computed by using the FFT programmes of Cooley and Tukey[22].

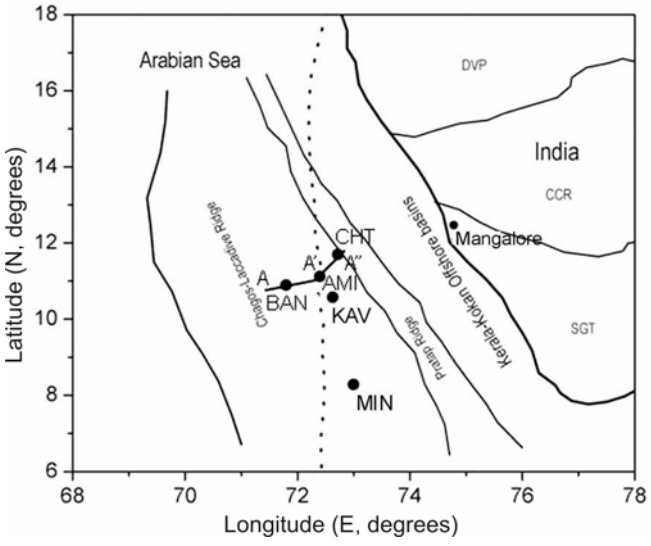

Figure 1. Map showing the trace of Reunion hotspot (dashed line) and Chagos–Laccadive Ridge in the central Indian Ocean formed during the transit of Indian Plate over it[48]. Tectonic and structural details for the western Indian shield and the offshore areas are adapted from refs 49–51. Lakshdweep group of islands that form the northern part of CLR and different GDS stations occupied during April–May 2004–05 are shown. Five different islands occupied are: MIN, Minicoy; KAV, Kavaratti; BAN, Bangaram; AMI, Amini; CHT, Chetalat; DVP, Deccan Volcanic Province; CCR, Central Cratonic Region; SGT, Southern Granulite Terrain; profile AA′A″ used for interpretation is also shown.

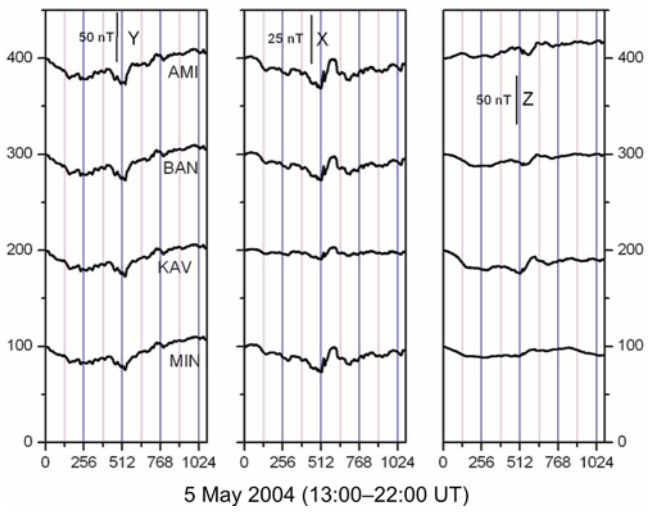

Figure 2. Magnetograms for the disturbed event recorded on 5 May 2004 (13:00–22:00 UT) at four different islands.

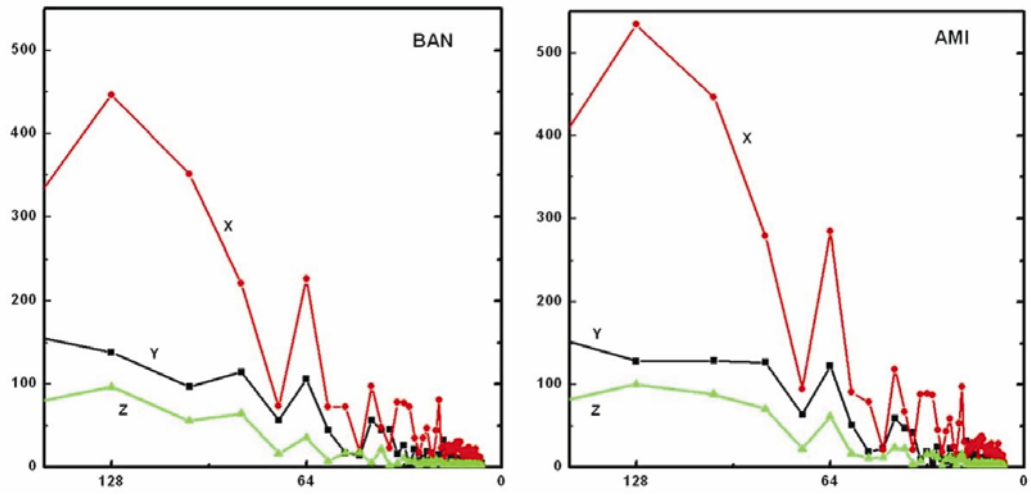

Figure 3. Fourier amplitude spectra for 2.5 h sequence of magnetic storm, 13:00–22:00 UT, on 5 May 2004, recorded at BAN and AMI.

Generally the transformation to the frequency domain is carried out according to the complex Fourier transform

$$g(\omega) = \int f(t) * \exp(-\mathrm{i}\omega t)\mathrm{d}t.$$

The Fourier spectra give the frequency content of time series data. The lower and upper frequency limits are set by length of data set and Nyquist frequency respectively. Magnetovariational data analysis is based on the Fourier components of X, Y and Z variations at different frequencies.

The amplitude spectra of each component are plotted against period (T) for BAN and AMI and are shown in Figure 3 for the substorm event recorded on 5 May 2004. Periods are selected at which one horizontal component (X) has a maximum value and other is reasonably stationary at a maximum or minimum value. In Figure 3, the peak values in X are observed at 64, 42, 34, 26 and 19 min periodicities.

Transfer functions

The main goal of processing technique is to transform magnetovariational data into frequency-dependent response functions symbolizing estimate of normalized anomalous field. This is achieved by calculating the transfer functions that show the relationship between anomalous and normal field components.

In practice, time-varying magnetic fields observed at any recording site can be considered to be composed of normal and anomalous parts[23]. If X_n, Y_n and Z_n and X_a, Y_a and Z_a represent the components of the normal and anomalous field respectively, then magnetic field components at any site (X_s, Y_s and Z_s) can be separated into normal and anomalous parts (e.g. $X_s = X_n + X_a$). In such a case, at a given site and for a given frequency interstation transfer functions that relate the anomalous and the normal field components can be expressed as:

$$\begin{bmatrix} X_a \\ Y_a \\ Z_a \end{bmatrix} = \begin{bmatrix} T_{xx} & T_{xy} & T_{xz} \\ T_{yx} & T_{yy} & T_{yz} \\ T_{zx} & T_{zy} & T_{zz} \end{bmatrix} \begin{bmatrix} X_n \\ Y_n \\ Z_n \end{bmatrix}.$$

The tensor (as shown in the equation) relating the anomalous and normal fields contains the nature of electrical conductivity distribution.

Under the assumption of uniform source field for short period fluctuations, when $Z_n \to 0$ and $Z_s \sim Z_a$, the vertical field transfer functions (T_{zx} and T_{zy}) can be expressed by a linear combination of two horizontal components

$$Z_a = Z_s = T_{zx}X_n + T_{zy}Y_n.$$

The magnitude of induction (real/quadrature) arrow is given by

$$S = \sqrt{(T_{zx}^2 + T_{zy}^2)}$$

and azimuth of the arrow

$$\Phi = \tan^{-1}(T_{zy} / T_{zx}).$$

Conventionally, the conductivity information contained in vertical transfer functions is extracted by presenting them as induction arrows. As a matter of convenience, the direction of real arrows is reversed so that they point towards regions of high electrical conductivity. Hence, when these arrows are displayed at all the sites, they form a powerful tool to locate and define the trend of the involved conductivity structures.

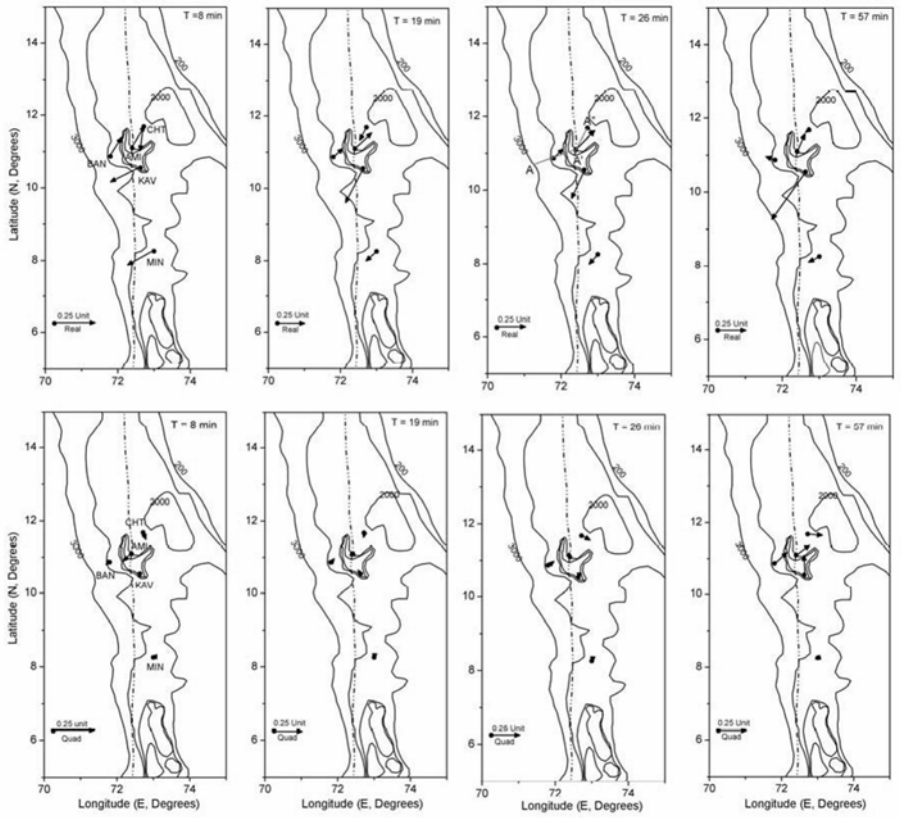

Figure 4. Observed induction arrows for 8, 19, 26 and 57 min (ref. 10). Notable point is that reversal between AMI and CHT in spite of seawater effect surrounding the islands. Line AA′A″ has been used for interpreting the geoelectric structure across CLR and is shown in T = 26 min.

We have selected local nighttime variations to ensure that the inducing field is uniform. The vertical field transfer functions are estimated by using 8–12 events (depending on data availability at each site). Using the given equation, the induction arrows were computed for the period range of 8–128 min using a robust technique[24] and are discussed here.

Induction arrows

The maps of observed induction arrows (for both real and quadrature; for periods 8, 19, 26 and 57 min) along with the bathymetry of the study area[10] are shown in Figure 4.

In spite of island effect (that is due to the sharp conductivity contrast between island and sea), the observed induction pattern at shorter periods (8–26 min) shows a reversal pattern between AMI and Chetalat (CHT). The induction pattern at BAN also points towards this region. This indicates a zone of current concentration along the track of CLR that is located between CHT and AMI. Thus at short periods, the induction pattern is dominated by the conductivity anomaly of the islands. At higher periods (34–57 min), the induction arrows point towards deep sea. The magnitudes of the NE oriented arrow diminish progressively with increasing periods, vanishing almost around 43 min. At still longer periods (shown only for 57 min), they rotate anti-clockwise and point towards the deep sea (where the water column has a thickness over 3 km). At Kavaratti (KAV) and MIN, the induction arrows point towards deep sea and CLR in southeast (SE) directions for all periods.

Hypothetical event analysis

Projecting the induction arrows on to the line of the transect of MV is carried out by the hypothetical event technique[25]. Hypothetical event analysis (HEA) is another form of depicting transfer functions in which the vertical field at all sites is computed with respect to external horizontal field of one unit with specified polarization. In an ideal 2-D case, the strongest response would be seen when the horizontal field is polarized at right angles to the strike, whereas the response would vanish for the orthogonal polarization uniform horizontal field of one unit with azimuth ϕ in clockwise direction with respect to north will induce currents such that its vertical field can be written as

$$Z_{\mathrm{r}} = (T_{zx})_{\mathrm{r}} * \cos\phi + (T_{zy})_{\mathrm{r}} * \sin\phi$$

$$Z_{\mathrm{i}} = (T_{zx})_{\mathrm{i}} * \cos\phi + (T_{zy})_{\mathrm{i}} * \sin\phi.$$

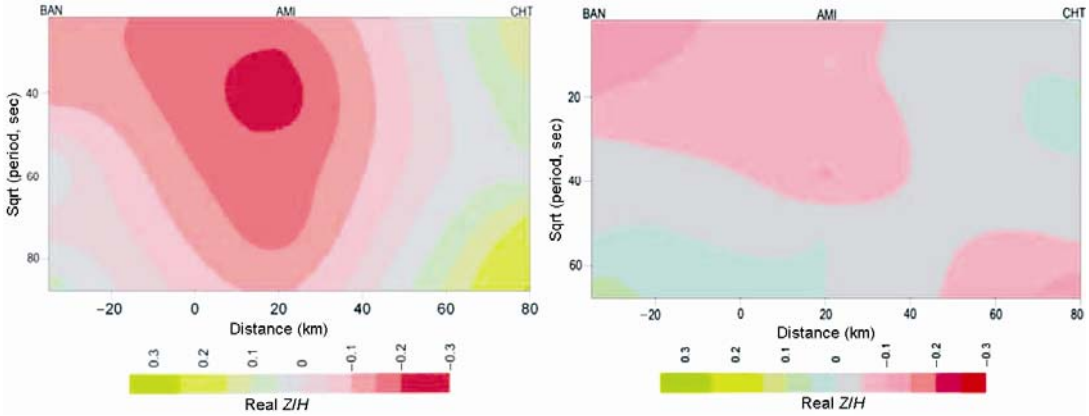

Figure 5. Pseudosection of real Z/H along profile AA′A″ brings out anomalous zone beneath AMI for N70°W polarization and the pattern diffuses for orthogonal polarization N20°E. Note that the vertical scale is square root of the time period.

The real (r) and imaginary (i) parts of the predicted anomalous response can be further combined to estimate modulus and phase of anomalous field

$$Z_{\mathrm{m}} = \sqrt{Z_{\mathrm{r}}^2 + Z_{\mathrm{i}}^2}$$

$$Z\phi = \tan^{-1}(Z_{\mathrm{i}}/Z_{\mathrm{r}}).$$

Ingham *et al.*[26] suggested an useful method of presentation of the transfer functions in terms of Z/H pseudosections. In this approach, if the values of Z_{r} or Z_{m} from a number of sites on a transverse are available at several periods, they can be contoured on a pseudosection for which the horizontal scale distance of sites along the traverse and the vertical scale is usually the square root of the period. This method, thus, serves as a qualitative guide to the variations of conductivity both with depth and along the line of sections.

Figure 5 shows the pesudosection for two mutually polarization angles corresponding to –70° and 20°. The pseudosection corresponding to –70° shows a low value of real Z/H at AMI. This feature is seen for lower periods and gets diffused for higher periods suggesting the shallow nature of the conductivity anomaly.

Though all stations have an island effect, this analysis has brought out the well defined conductivity anomaly beneath AMI corresponding to a polarization of N70°W and for orthogonal polarization of N20°E, the pattern almost diffuses. This suggests that the anomaly is largely 2-D in nature.

Long period magnetotelluric sounding

Magnetotelluric sounding provides a way to determine the electrical conductivity image of the subsurface by simultaneous measurement of natural electric and magnetic field variations[27]. For a general 3-D variation, horizontal electric (E_x, E_y) and magnetic (H_x, H_y) field at a given frequency are related through

$$\begin{pmatrix} E_x \\ E_y \end{pmatrix} = Z \begin{pmatrix} H_x \\ H_y \end{pmatrix},$$

where Z (impedance tensor) is a complex tensor in frequency domain

$$Z = \begin{pmatrix} Z_{xx} & Z_{xy} \\ Z_{yx} & Z_{yy} \end{pmatrix}.$$

Apparent resistivity and phases are computed as

$$\rho_{ij} = \frac{1}{\omega\mu} | Z_{ij} | 2$$

$$\phi_{ij} = \arctan(\mathrm{Im}(Z_{ij})/\mathrm{Re}(Z_{ij})),$$

where $i = 1, 2$ and $j = 1, 2$.

For subsurface geoelectrical mapping, three long period magnetotelluric (LMT) sounding units and five GDS stations were operated at different islands. Data from two LMT and GDS units were lost due to the encroachment of seawater during a cyclonic storm. We present representative results from the LMT site CHT. Figure 6 shows the apparent resistivity (ρ_{xy} and ρ_{yx}) and phases (Φ_{xy} and Φ_{yx}) from 10 to 16,000 S along with the 1-D conductivity structure. This conductivity–depth profile suggests that the top layer is a sedimentary layer extending up to a depth of about 6–8 km, presence of high conductivity layer at 18–22 km depth and a possible lithosphere-boundary at a depth of about 70 km. The presence of a high conductivity layer at midcrustal depth suggests rheological stratification and marks the onset of ductile behaviour. This layer arises due to the presence of fluids trapped beneath the impermeable layer[28,29]. It is

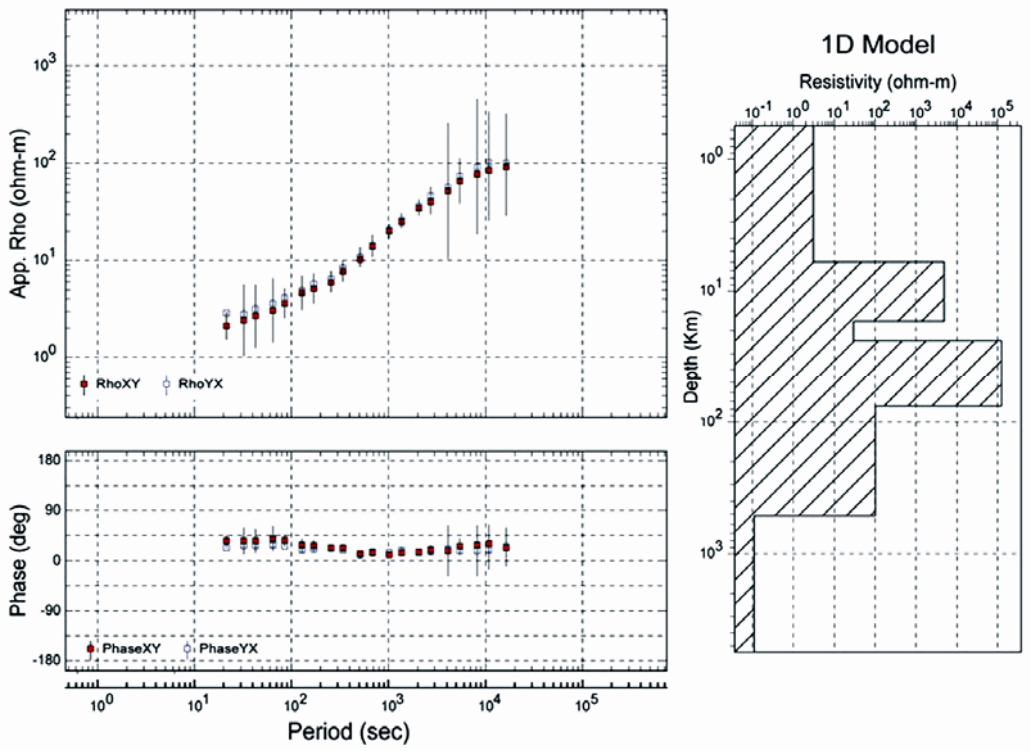

Figure 6. Apparent resistivity (ρ_{xy} and ρ_{yx}) and phases (Φ_{xy} and Φ_{yx}) curves for the LMT site CHT. One-dimensional resistivity depth section for different resistivity structure along two measurement directions (N–S and E–W) is shown.

believed that these fluids may be produced by thermally controlled ametamorphic dehydration process[30,31].

Modelling

Thin-sheet modelling

In regional scale studies like induction in the vicinity of the islands, coastlines, channels, etc., the charge collected at conductivity discontinuity cannot be neglected and current flowing in and out of the thin sheet must be considered, i.e. formulation should include both poloidal and toroidal modes. Thus, the geological structure of Lakshdweep group of islands is complex that it cannot be approximated to a 2-D structure. Numerical solution of 3-D structures is limited in the literature. This is due to large computer storage and computational time that solution of Maxwell's equations requires for a reasonable approximation. However, if conductivity anomalies are confined to a surficial layer and having a thickness much smaller than the skin depth of the underlying medium, the computational procedure can be greatly simplified by replacing the non-uniform layer as a thin sheet of variable conductance[32]. Later, Price has pointed out that charges collected at conductivity discontinuities are bound to affect the local electric field[33]. We have adopted 3-D thin-sheet modelling developed by Vasseur and Weidelt[34] for calculating the shielding effect due to seawater and sedimentary basin.

The limit on the thickness of the sheet is provided by the conductivity of the material constituting the sheet as well as by the linked electrical substratum so that, at the periods of investigation, the horizontal field remains constant over the thickness of the sheet[7,35]. This implies that the thickness of the sheet should be small compared to the skin depth of the diffusing electromagnetic (EM) wave, in the layer immediately beneath the sheet, at a considered period. A second condition is that the sheet thickness should be very small in relation to the skin depth in any material included in the sheet. In numerical grid, node spacing should not be greater than one-third of the skin depth of the layer underlying the thin sheet. The thin sheet was assigned a thickness of 6 km that allows incorporating bathymetry (depth of seawater column) as well as sedimentary basin of the study region. This thin sheet layer was considered to overlie a three-layered structure having a resistivity of 200, 1000 and 50 Ωm with a thickness of about 20 and 50 km is considered to overlie a half space of about 50 Ωm. The choice of the background-layered structure was based on the geoelectrical model obtained from CHT results.

The skin depth of the underlying layer for 19 min is about 240 km and is much larger than the assumed thickness (6 km) of the anomalous surface layer. Similarly, the skin depth of the seawater is approximately 10 km, again

about 3–4 times larger than the maximum depth of the seawater. Thus, the thin sheet conditions[35] are met everywhere. The grid spacing is 25 km and satisfies the condition that it should be less than one-third of the skin depth of the underlying layer. Thus the thin sheet satisfies the conditions necessary to validate the thin sheet approximation as described earlier.

For the purpose of numerical computation, an area of 5°–15°N and 71°–80°E was chosen and divided into 50×50 grid with a grid interval of 25 km, i.e. one order less than the skin depth of the underlying layer beneath the thin sheet. The computations have been carried out for a period of 8–128 min. For calculating the island effect, the thickness of the water column has been adopted from the bathymetry maps published by the Naval Hydrographic Office[36] and thickness of the sedimentary basin from isopach map of Arabian Sea[37] as well as from the gravity modelling carried out by Radha Krishna *et al.*[16]. Resistivities of 10 and 50 Ωm have been adopted for layers I and II from LMT results. The conductivity of seawater was taken to be 0.33 Ωm (ref. 38). Conductance map of Lakshdweep and surrounding region is shown in Figure 7. The above thin sheet was considered to be overlain by 1-D structure as discussed in LMT section. The shielding effect obtained from these calculations is shown in Figure 8.

2-D Modelling

Data regarding the electrical conductivity distribution beneath the subsurface are extracted from the induction responses at different frequencies by numerical modelling. The numerical modelling is carried out by finite difference (FD), finite element (FE) and integral equation

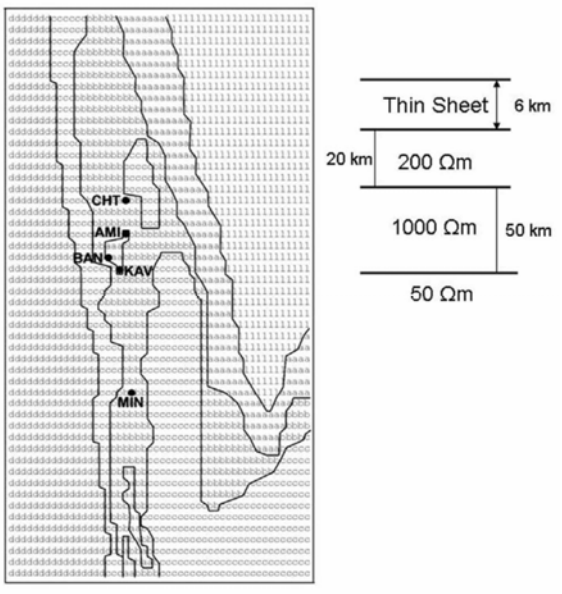

Figure 7. Conductance codes depicting distribution of conductance values in the thin-sheet model for Lakshdweep and surrounding regions. One-dimensional structure beneath thin sheet is also shown. Magnetometer sites are marked by solid circles. Conductance codes used are lllll 30 S, aaaaa 1160 S, bbbbb 3700 S, ccccc 7000 S, ddddd 10100 S.

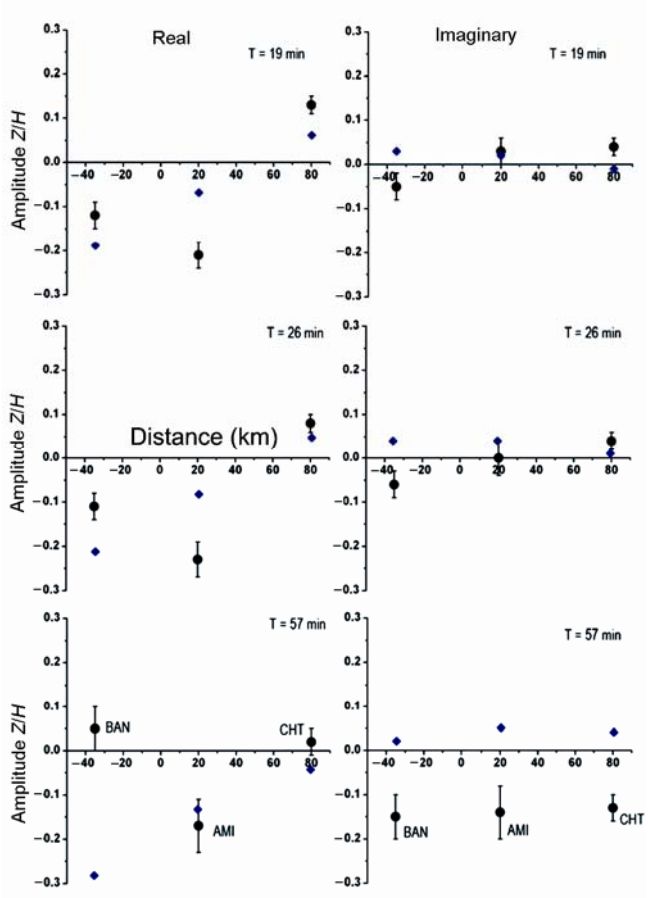

Figure 8. Comparison between observed induction pattern (dot) and calculated shielding effects due to variations in the seawater column with sedimentary basin together (blue-diamond) are shown for three different periodicities.

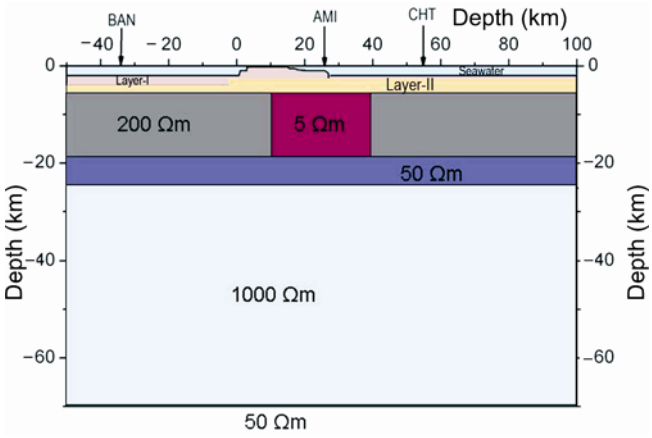

Figure 9. The geoelectric crustal model across northern part of CLR (Lakshdweep group of islands) brings out midcrustal conductivity anomaly associated with Reunion hotspot activity when Indian plate has moved over it. Layers I and II correspond to unconsolidated and consolidated sedimentary layers.

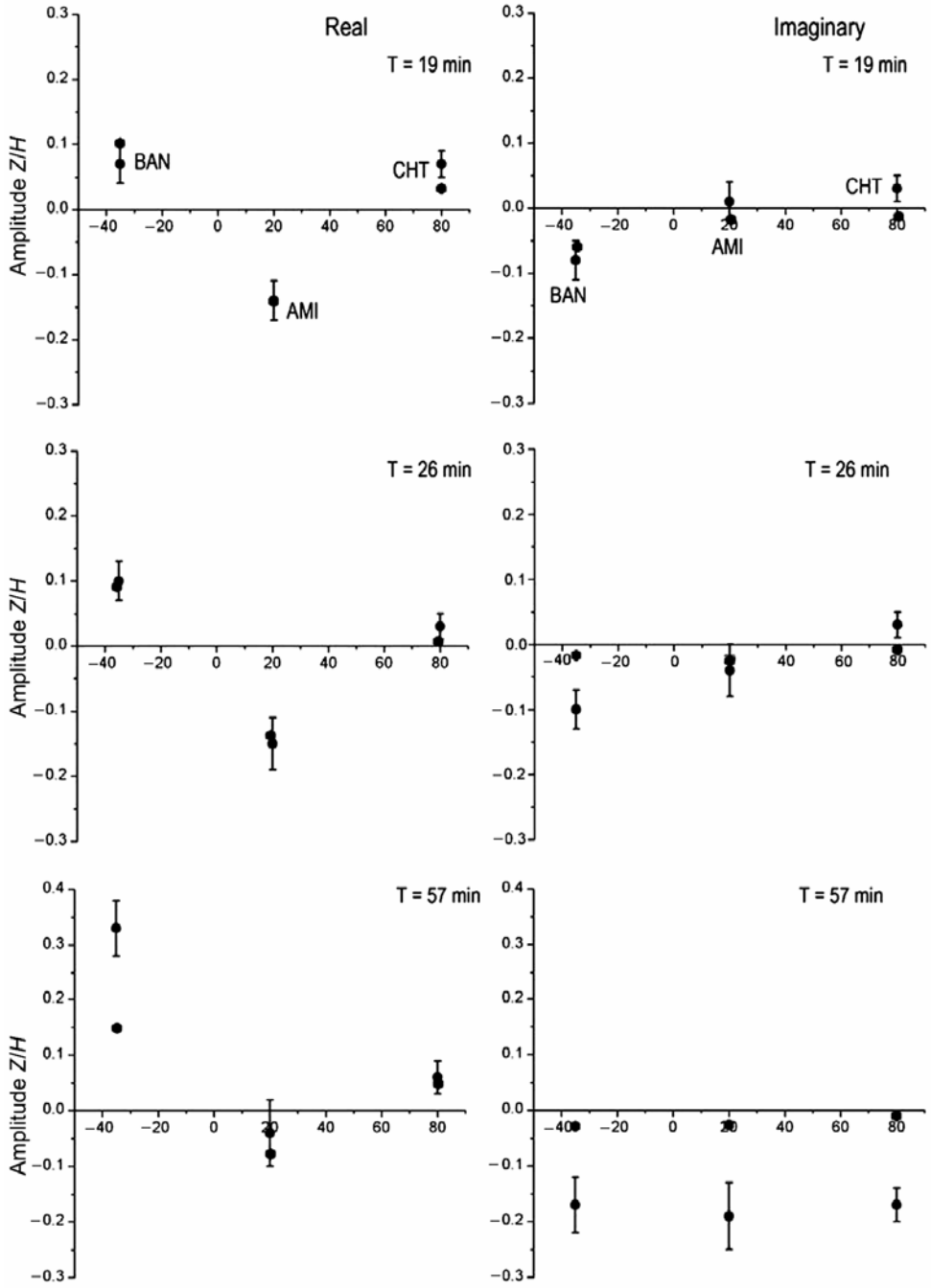

Figure 10. Residual induction arrows obtained after eliminating the seawater column and sedimentary basin effect (black circle) for three different periods. Pentagon denotes the computed values for the model shown in Figure 9.

(IE) methods. IE codes have been mainly used to model the responses from finite bodies, whereas the FD and FE codes have been developed for general varying subsurface conductivity. We have adopted 2-D FD algorithm developed by Cerv *et al*. for estimating the electrical conductivity distribution beneath the Lakshdweep region[39]. In this method, Maxwell's equations are solved by representing the differential equations and boundary conditions in the form of FDs between field values at adjacent points on a 2-D grid superimposed on the conductivity distribution. In the procedure of forward modelling, after defining the model parameters, the response function is computed and compared with the observed one. Thereafter, the parameters of the model or the model itself are changed until a satisfactory fit is found between the computed and the observed response. For 2-D modelling, the total length of the selected profile is 150 km with a node spacing of about 3 km. For eliminating the edge effects

(i.e. boundary effects), the grid spacing is extended to sufficiently larger distances away from the observational domain. The residual induction arrows obtained after eliminating island effect from observed have been modelled and discussed here.

For modelling purpose, the anomalous vertical field (Z_r and Z_i) defined along the profile AA′A″ running perpendicular to the strike were used to develop the geoeletrical model. The anomalous vertical fields were generated from transfer functions by application of HEA for a polarization of horizontal field which maximizes the induction.

Two-dimensional modelling was carried out for 19 min as the induction arrows acquire a peak value at this periodicity. The thickness of the lithosphere adopted in the present study is about 70 km and the distribution of the electrical resistivity values adopted in the 2-D-model was based on LMT results from CHT. This result suggests that lithosphere–asthenosphere boundary at 70 km (having resistivity of about 1000 Ωm) with the half-space of 50 Ωm below asthenosphere. The lithosphere thickness obtained from LMT results correlates very well with the shear wave velocity structure[40,41] and gravity studies carried out by Radha Krishna *et al.*[16]. These studies suggest that the thickness of the lithosphere beneath CLR is about 70–80 km.

As the shielding effect due to seawater layer and sediments has been eliminated, the residual induction arrows have been modelled by replacing them with a land material simulated by resistivity of 200 Ωm. The residual induction pattern has been explained in terms of high conductivity anomaly underlying AMI and extending towards BAN as shown in Figure 9. Comparison between residual and calculated induction pattern is also shown in Figure 10. The reliability of the model was tested by comparing the residual induction and calculated response at a period of 19 min and two additional periods of 26 and 57 min. The possible cause for this high conductivity anomaly is discussed here.

Results and discussions

Suppression of induction arrows at AMI and reversal between BAN and CHT suggests the concentration of anomalous induced currents in an elongated structure corresponding with the track of the Reunion hotspot. This has been reflected as an anomalous conductivity zone at a depth of about 3–16 km along the track of Reunion hotspot from the 2-D modelling carried out across the Lakshdweep group of islands (northern part of CLR). This zone may represent the underplating mantle material related to the Reunion hotspot volcanism.

Movement of Indian lithosphere plate over Reunion mantle plume produced a chain of volcanic islands (Laccadive and Maldive Islands) during 45–60 Ma (ref. 42). Thermal remobilization/reactivation during this period may have increased the mantle temperature beneath the CLR[43]. Progressive adiabatic melting in the upper mantle leads to large volumes of magma that are partially erupted/intruded at the earth's surface[44,45]. This is reflected as high-density mantle material underplating beneath CLR from gravity studies carried out by Singh[46], Ashalatha *et al.*[47] and Radha Krishna *et al.*[16]. This thermal reactivation may trigger and release hydrous fluids/volatiles that could be a source for high conductivity anomaly observed beneath CLR. This is reflected as a low velocity zone (15–25 km) mapped by Manglik[41] using shear wave velocity. The zone of low seismic velocity, high mantle temperature and underplating mantle material beneath CLR is not necessarily coincident with depth and may symbolize partial melt of crustal and mantle material associated with the hotspot volcanism. Thus, the anomalous conductivity layer may represent a underplated magma chamber of basic composition which becomes ponded at or near the crust/mantle following their ascent through the mantle related to hotspot volcanism.

Conclusions

Midcrustal conductivity anomaly has been identified in Lakshdweep Islands (northern part of CLR). However, the deep structure of CLR still remains elusive. New seafloor EM measurements in this region supplemented by LMT soundings over Lakshdweep Islands will be useful in determining the electrical conductivity distribution for the evolution of northern part of CLR.

1. Morgan, W. J., Convection plumes in the lower mantle. *Nature*, 1971, **230**, 42–43.
2. Morgan, W. J., Plate motions and deep mantle convection. *Mem. Geol. Soc. Am.*, 1972, **132**, 7–22.
3. Gough, D. I. and Ingham, M. R., Interpretation methods for magnetometer arrays. *Rev. Geophys. Space Phys*., 1983, **21**, 141–157.
4. Arora, B. R., Geomagnetic depth sounding. In *Natural Source Electromagnetic Induction in the Earth* (eds Arora, B. R. and Srinivas), New Age International Limited Publishers, New Delhi, 1997, pp. 80–128.
5. Nityananda, N., Agarwal, A. K. and Singh, B. P., Induction at short period on the horizontal field variation in the peninsular India. *Phys. Earth Planet. Inter*., 1997, **15**, 5–9.
6. Thakur, N. K., Mahashabde, M. V., Arora, B. R., Singh, B. P., Srivastava, B. J. and Prasad, S. N., Geomagnetic variation anomalies in peninsular India. *Geophys. J. R. Astron. Soc.*, 1986, **86**, 839–854.
7. Agarwal, A. K. and Weaver, J. T., Regional electromagnetic induction around the Indian peninsula and Sri Lanka; a three-dimensional numerical model study using the thin sheet approximation. *Phys. Earth Planet. Inter*., 1989, **54**, 320–331.
8. Arora, B. R. and Subba Rao, P. B. V., Integrated modeling of EM response functions from peninsular India and Bay of Bengal. *Earth Planets Space*, 2002, **54**, 637–654.
9. Fisk, M. R. *et al*., Reunion hotspot magma chemistry over the past 65 Ma: results from Leg 115 of the Ocean Drilling Program. *Geology*, 1989, **17**, 934–937.

10. Subba Rao, P. B. V. and Arora, B. R., Magnetovariational study over Lakshadweep Islands, southwestern continental margin of India. *Curr. Sci.*, 2007, **92**, 1767–1773.
11. Naini, B. R. and Talwani, M., Structural framework and evolutionary history of the continental margin of western India. In *Studies in Continental Margin Geology* (eds Wakins, J. S. and Drake, C. L.), Am. Assoc. Pet. Geol. Mem, 1982, vol. 34, pp. 167–191.
12. Ben Avraham, Z. and Bunce, E. T., Geophysical studies of the Chagos–Laccadive Ridge, Indian Ocean. *J. Geophys. Res.*, 1977, **82**, 1295–1305.
13. Harbison, R. N. and Bassinger, B. G., Marine geophysical studies off western India. *J. Geophys. Res.*, 1973, **78**, 432–440.
14. Fisher, R. L., Sclater, J. G. and Mckenzie, D. P., Evolution of the central Indian ridge, western Indian Ocean. *Bull. Geol. Soc. Am.*, 1971, **82**, 553–562.
15. Mckenzie, D. and Sclater, J. G., The evolution of the Indian Ocean since the late Cretaceous. *Geophys. J. R. Astron. Soc.*, 1971, **25**, 437–528.
16. Radha Krishna, M., Verma, R. K. and Purushotham, A. K., Lithospheric structure below the eastern Arabian Sea and adjoining west coast of India based on integrated analysis of gravity and seismic data. *Mar. Geophys. Res.*, 2002, **23**, 25–42.
17. Duncan, R. A., Hotspots in the Southern Oceans – an absolute frame of reference for motion of the Gondwana continents. *Tectonophysics*, 1981, **74**, 29–42.
18. Morgan, W. J., In *The Sea: The Oceanic Lithosphere* (ed. Emiliani), Wiley-Interscience, New York, 1981, vol. 7, pp. 443–487.
19. Duncan, R. A., In Proceedings of the Ocean Drilling Program, Scientific Results (eds Duncan, R. A. *et al.*), College Station, Texas, 1990, vol. 115, pp. 3–10.
20. Banks, R. J., Data processing and interpretation in geomagnetic depth sounding. *Phys. Earth Plannet. Inter.*, 1973, **7**, 339–348.
21. Lilley, F. E. M., Electrical conductivity anomalies and continental seismicity in Australia. *Nature*, 1975, **257**, 381–382.
22. Cooley, J. W. and Tukey, J. W., An algorithm for the machine calculation of complex Fourier series. *Math. Comput.*, 1965, **19**, 297–301.
23. Schmucker, U., Anomalies of geomagnetic variations in the southwestern United States. *Bull. Scripts Inst. Oceanogr.*, 1970, **13**, 1–165.
24. Egbert, G. D. and Booker, J. R., Imaging crustal structure in Southwestern Washington with small magnetometer arrays. *J. Geophys. Res.*, 1993, **98**, 15967–15985.
25. Bailey, R. C., Edwards, R. N., Garland, G. D. and Greenhouse, J. P., Electrical conductivity studies over a tectonically active region in eastern Canada. *J. Geomag. Geoelec.*, 1974, **26**, 125–146.
26. Ingham, M. R., Bhingam, D. K. and Gough, D. I., Magnetovariational study of a geothermal anomaly. *Geophys. J. R. Astron. Soc.*, 1983, **72**, 597–618.
27. Vozoff, K., The magnetotelluric method in the exploration of sedimentary basins. *Geophysics*, 1972, **37**, 98.
28. Muir-Wood, R. and King, G. C. P., Hydrological signatures of earthquake strain. *J. Geophys. Res.*, 1993, **98**, 22035–22068.
29. Jones, A. G., MT and reflection: an essential combination. *Geophys. J. R. Astron. Soc.*, 1987, **89**, 7–18.
30. Fyfe, W. S., Price, N. J. and Thompson, A. B., *Fluids in the Earth's Crust*, Elsevier, Amsterdam, 1978, pp. 1–383.
31. Bailey, R. C., Trapping of aqueous fluids in the deep crust. *Geophys. Res. Lett.*, 1990, **17**, 1129–1132.
32. Price, A. T., The induction of electric currents in non-uniform thin sheets and shells. *Q. J. Mech. Appl. Math.*, 1949, **2**, 283–310.
33. Price, A. T., The theory of geomagnetic induction. *Phys. Earth Planet. Inter.*, 1973, **7**, 227–273.
34. Vasseur, G. and Weidelt, P., Bimodal electromagnetic induction in non-uniform thin sheets with an application to the northern Pyrenean induction anomaly. *Geophys. J. R. Astron. Soc.*, 1977, **51**, 669–690.
35. Weaver, J. T., Regional induction in Scotland; an example of three-dimensional numerical modeling using the thin sheet approximation. *Phys. Earth Planet. Inter.*, 1982, **28**, 161–180.
36. NHO, Bathymetry map of Bay of Bengal, Superintendent, Naval Hydrographic Office, Dehradun, India, 1977.
37. Balakrishnan, T. S., Major tectonic elements of the Indian subcontinent and contiguous areas: a geophysical view. *Mem. Geol. Soc. India*, 1997, **38**, 155.
38. Heinson, G. S. and Lilley, F. E. M., An application of thin sheet electromagnetic modeling to the Tamsan Sea. *Phys. Earth Planet. Inter.*, 1993, **81**, 231–251.
39. Cerv, V., Pek, J. and Praus, O., Numerical modeling of geoelectrical structures in Czechoslovakia. *Phys. Earth Planet. Inter.*, 1987, **45**, 170–178.
40. Singh, D. D., Q-structure beneath the north and central Indian Ocean from the inversion of the observed Love and Rayleigh wave attenuation data. *Phys. Earth Planet. Inter.*, 1990, **59**, 243–258.
41. Manglik, A., Shear wave velocity structure of the upper mantle under the NW Indian Ocean. *J. Geodyn.*, 2002, **34**, 615–625.
42. Vandamme, D. and Courtillot, V., Palaeomagnetism of Leg 115 basement rocks and latitudinal evolution of the Réunion hotspot. *Proc. ODP Sci. Results*, 1990, **115**, 111–117.
43. Henstock, T. J. and Thompson, P. T., Self-consistent modeling of crustal thickness at Chagos–Laccadive ridge from bathymetry and gravity data. *Earth Planet. Sci. Lett.*, 2004, **224**, 325–336.
44. Condie, K. C., *Plate Tectonics and Crustal Evolution*, Pergamon Press, 1989, pp. 1–469.
45. Caress, D. W., McNutt, M. K., Detrick, R. S. and Mutter, J. C., Sediment imaging of hot-spot related crustal underplating beneath the Marquesas Islands. *Nature*, 1995, **373**, 600–603.
46. Singh, A. P., Deccan volcanism on deep crustal structure along western part of Indian mainland and adjoining Arabian Sea. *Curr. Sci.*, 2002, **82**, 316–325.
47. Ashalatha, B., Subrahmanyam, C. and Singh, R. N., Origin and emplacement of Chagos–Laccadive Ridge, Indian Ocean, from admittance analysis of gravity and bathymetry data. *Earth Planet. Sci. Lett.*, 1991, **105**, 47–54.
48. Richards, M. A., Duncan, R. A. and Courtillot, V., Flood basalts and hot spot tracks: plume heads and tails. *Science*, 1989, **246**, 103–107.
49. Biswas, S. K., Rift basins in western margin of India and their hydrocarbon prospects with special reference to Kutch basin. *Am. Assoc. Pet. Geol. Bull.*, 1982, **64**, 209–220.
50. Biswas, S. K., Regional tectonic framework, structure and evolution of the western marginal basins of India. *Tectonophysics*, 1987, **135**, 307–327.
51. Subrahmanyam, V., Gopala Rao, D., Ramana, M. V., Krishna, K. S., Murthy, G. P. S. and Gangadhara Rao, M., Structure and tectonics of the southwestern continental margin of India. *Tectonophysics*, 1995, **249**, 267–282.

ACKNOWLEDGEMENTS. We thank Department of Science and Technology, New Delhi, for funding our project. The logistics provided by local Department of Science and Technology, Lakshdweep Islands is gratefully acknowledged. We thank Prof B. R. Arora and Dr C. D. Reddy for fruitful suggestions. Review by Dr Nandini Nagarajan, NGRI, Hyderabad is gratefully acknowledged. We also thank Mr D. M. Daga for the assistance provided in the fieldwork. We are grateful to Prof. A. Bhattacharyya, Director, Indian Institute of Geomagnetism, for her kind encouragement to carry out this work.

Received 10 October 2008; revised accepted 23 April 2010